

RESEARCH

Open Access



Unique transcriptomic responses of rat and human alveolar macrophages in an in vitro model of overload with TiO₂ and carbon black

Laetia Perez^{1*}, Jérôme Ambroise², Bertrand Bearzatto², Antoine Froidure^{3,4}, Charles Pilette^{3,4}, Yousof Yakoub¹, Mihaly Palmay-Pallag⁵, Caroline Bouzin⁶, Laurence Ryelandt⁷, Cristina Pavan⁸, François Huaux¹ and Dominique Lison¹

Abstract

Background Chronic inhalation of titanium dioxide or carbon black can lead, at high exposure, to lung overload, and can induce chronic inflammation and lung cancer in rats. Whether this rat adverse response is predictive for humans has been questioned for more than 40 years. Currently, these particles are conservatively considered as *possible* human carcinogens.

Objective To clarify the mechanisms of the adverse rat response to lung overload and its human relevance.

Methods Primary rat and human alveolar macrophages were exposed in vitro to control, non-overload or overload doses of titanium dioxide (P25) or carbon black (Printex 90) particles, and their activation profile was examined by untargeted transcriptomics.

Results Rat macrophages were largely the most responsive to particle overload. In particular, eighteen genes were identified as robust markers of P25 and Printex 90 overload in rat cells. The known functions of these genes can be related to the potential mechanisms of the adverse outcomes recorded in rats in vivo. Most of these 18 genes were similarly modulated in human macrophages, but with a markedly lower magnitude. In addition, a 16 gene signature was observed upon overload in human macrophages, but not in rat macrophages.

Conclusions These findings provide insights into the mechanisms of lung overload and inflammation in rats, and highlight similarities and differences in transcriptomic responses of rat and human alveolar macrophages.

Keywords Occupational lung diseases, Species comparison, Alveolar macrophages, Particle overload, Omics

*Correspondence:

Laetia Perez
laetia.perez@uclouvain.be

Full list of author information is available at the end of the article



© The Author(s) 2025. **Open Access** This article is licensed under a Creative Commons Attribution-NonCommercial-NoDerivatives 4.0 International License, which permits any non-commercial use, sharing, distribution and reproduction in any medium or format, as long as you give appropriate credit to the original author(s) and the source, provide a link to the Creative Commons licence, and indicate if you modified the licensed material. You do not have permission under this licence to share adapted material derived from this article or parts of it. The images or other third party material in this article are included in the article's Creative Commons licence, unless indicated otherwise in a credit line to the material. If material is not included in the article's Creative Commons licence and your intended use is not permitted by statutory regulation or exceeds the permitted use, you will need to obtain permission directly from the copyright holder. To view a copy of this licence, visit <http://creativecommons.org/licenses/by-nc-nd/4.0/>.

Background

The extensive production and use of titanium dioxide (TiO₂) or carbon black (CB) particles in a large variety of commercial products may result in significant inhalation exposure in occupational settings [1, 2]. The toxicity of these particles was initially not of great concern because both TiO₂ and CB are considered as poorly soluble and low toxicity particles (PSLT), and had regularly been used as negative controls in experimental lung toxicity studies. However, about 40 years ago, chronic inflammatory and carcinogenic lung responses were recorded in experimental rats after chronic inhalation of high doses of TiO₂ or CB particles [3–5], thus raising new concerns about the hazard to which occupational populations may be exposed.

The adverse effects of PSLT in rats have been mechanistically linked to lung particle overload, which, based on in vivo studies, is supposed to be initiated when the pool of alveolar macrophages (AM) has accumulated, on average, a volume of particles over 6% of their total cellular volume [6]. This percentage corresponds to a particle volume of approximately 60 μm³/AM, which was further extended to a range of 25 to 90 μm³/AM [7]. Under these overload conditions, the clearance capacity of AM is impaired, and PSLT accumulate in the lung [6, 8]. In rats, lung overload induced by PSLT exposure can then drive a persistent neutrophilic inflammation, oxidative stress, fibrosis, type II epithelial cell hyperplasia, metaplasia and, in turn, lung cancer [8–10]. While lung overload has been observed in several experimental species (rat, mouse, hamster, monkey) exposed to PSLT, severe adverse outcomes have only been recorded in the rat [3–5, 11–13]. The precise molecular mechanisms underlying these responses remain poorly understood.

Whether the rat adverse response to PSLT is relevant to predict a hazard for humans exposed to high doses of these particles is still a source of debate 40 years later. Epidemiological studies have not demonstrated evidence of an increased risk of lung disease in occupational cohorts exposed to TiO₂ or CB [14]. However, in view of inadequate evidence in humans and sufficient evidence from rodent studies, the International Agency for Research on Cancer (IARC) has classified these particles as “possibly carcinogenic to humans” [15]. Further epidemiological research cannot contribute to refine this hazard assessment, as adequate cohorts exclusively exposed to TiO₂ or CB levels leading to lung overload, are unlikely to be available. In vitro studies using human AM might thus be an appropriate way forward.

Previous research has demonstrated the potential of in vitro models to predict human toxicity. For example, a comparative study using both rat and human in vitro airway epithelial models showed good concordance in predicting the toxicity of 14 reference chemicals, aligning

well with the results of in vivo acute rat toxicity studies [16]. Similarly, a “parallelogram approach” comparing gene expression changes in human and rat hepatocytes in vitro with rat liver in vivo identified key biological pathways consistently disrupted in all three systems, highlighting the potential of this approach to predict human liver toxicity [17].

In the present study, we hypothesized that AM exposed to high levels of PSLT particles, expected to cause overload in vivo, undergo phenotypic changes associated with transcriptomic dysregulations that promote chronic inflammatory and carcinogenic lung responses in rats. To investigate the human relevance of the adverse rat responses, we exposed primary AM from rats or humans in vitro to control, non-overload or overload doses of TiO₂ (P25) or CB (Printex 90) particles. After exposure, gene expression was analyzed and the transcriptomic profiles in each species were compared. Overload conditions were defined based on Morrow hypothesis of internalized particle volume and will be described herein as “AM overload”.

Methods

Particle dispersion in culture medium

TiO₂ (P25, a mixture of 80% anatase / 20% rutile), and CB (Printex 90) particles were provided by the Titanium Dioxide Manufacturers Association (TDMA, Brussels, Belgium) and the International Carbon Black Association (ICBA, New Orleans, USA), respectively. Since particle size is an important aspect in inhalation toxicology, a dispersion protocol was developed to obtain the same granulometry as in in vivo studies that recorded adverse outcomes [3, 4]. Prior each experiment, P25 and Printex 90 particles were weighed, heated 2 h at 200 °C to inactivate any microbial contaminants, suspended in complete culture medium (see AM culture below) to achieve a stock concentration of 5 mg/mL and dispersed with a VCX-750 probe sonicator (Sonics & Materials, Connecticut, USA) at 750 W, 40% amplitude and 0 pulse during 20 s. Suspensions of P25 particles were then vortexed for a few seconds.

Particle characterization

Morphology and specific surface area of the particles were assessed on the powder product by scanning electron microscopy (ultra 55 FegSEM, Carl Zeiss, Oberkochen, Germany) and N₂ adsorption (BET method), respectively. Particle size and effective density of the dispersed particles were measured by HELOS laser diffraction (Sympatec GmbH, Etten-Leur, Netherlands) and by the volumetric centrifugation method established by DeLoid, Cohen, Pyrgiotakis and Demokritou [18], respectively. The physicochemical characteristics of P25 and Printex 90 particles are reported in Table S2. Particle

size distributions following dispersion are shown in Supplemental data Figure S1.

Broncho-alveolar lavage collection

Eight-week-old male F344/HanZtmRj rats were purchased from Janvier Labs (St Berthevin, France) and were housed in individually ventilated cages in a controlled environment (21.3 ± 0.4 °C, $53.4 \pm 8.9\%$ relative humidity, 16 h light/8 h dark cycle, with water containing 4 ppm chlorine (hydropac-pouches from Plexx, Gelderland, Netherlands) and food *ad libitum*) at the IREC animal facility (UCLouvain, Brussels, Belgium). Twenty-eight (first RNA-seq experiment), 12 (second RNA-seq experiment) or 10 (RT-qPCR) rats were euthanized with an intraperitoneal injection of 1mL of 60 mg/mL pentobarbital. Vena cava was then incised to bleed the animals and the trachea was cannulated. Lung perfusion was performed by injecting 20mL of NaCl 0.9% into the right ventricle to flush circulating blood cells. Broncho-alveolar lavages were then collected by using 10mL pre-warmed (37 °C) phosphate buffered saline (PBS) supplemented with 1% Fetal Bovine Serum (FBS) and 1mM ethylenediaminetetraacetic acid (EDTA).

Human AM were obtained by broncho-alveolar lavage from 3 healthy (non-smoking male students aged 20–25 years) without evidence or history of chronic respiratory condition, at the Cliniques Universitaires Saint-Luc (Brussels, Belgium). The healthy volunteers were lightly sedated by intravenous injection of midazolam (1 to 3 mg), and the upper airways were anaesthetized with a lidocaine spray. Broncho-alveolar lavages were then collected from the middle lobe using 4×50 mL pre-warmed (37 °C) sterile saline, which were pooled for each individual.

AM culture

After collection, broncho-alveolar lavages were centrifuged 10 min at 300 g at room temperature. Pelleted cells from both species were suspended in complete cell culture medium composed of Dulbecco's modified Eagle medium (DMEM) supplemented with 10% Fetal Bovine Serum (FBS) and 1% Antibiotic-Antimycotic (AA) (quoted complete culture medium), pooled (for rat RNA-seq analyses) and counted in an aliquot containing Trypan blue solution. Concentration of 200.000 cells/mL were then achieved and 100.000 cells/cm² culture well surface area were added to a 96- or a 48-well culture plate, i.e. 30.000 cells/well for 96-well culture plate and 100.000 cells/well for 48-well culture plate. Cells were kept in a CO₂ incubator for 5 days prior to exposure. Each experiment included specific plates for determining non-overload and overload doses, measuring cytotoxicity dose-responses, and collecting RNA.

Experimental strategy

Before performing the RNA-seq experiments, we completed a series of preliminary experiments with rat AM to carefully select culture conditions, exposure doses, and cytotoxic activity (Fig. 1A-C and Table S1). Next, we verified that these parameters were also valid for human AM.

First, we noted that, after overnight culture, AM were rounded and did not adhere well to the wells. We extended the culture period prior to exposure, and found that, after 5 days (with culture medium changed after 2 or 3 days), AM adhered strongly and had developed pseudopods (Fig. 1A). Thus, we pre-cultured AM for 5 days prior to PSLT exposure in all experiments.

In order to verify that the RNA-seq analyses be conducted at non-cytotoxic doses, rat and human AM were cultured for 5 days in a 96-well culture plate (Greiner Bio-One, Kremsmünster, Austria) and then exposed for 4 days to 150 µL of increasing doses (from 0 to 50 µg/mL) of P25 or Printex 90 particles suspended in complete culture medium. The dose-response relationship for cytotoxicity was assessed with a water-soluble tetrazolium salt (WST)-1 assay (5%, Roche, Basel, Switzerland) following the manufacturer's guidelines (Fig. 1B). The data were analyzed by a two-way ANOVA followed by a post-hoc Dunnett test (treatment vs. control) using GraphPad Prism 9.4.1. Differences with p-value < 0.05 were considered statistically significant.

Next, we determined the nominal doses of PSLT needed (µg/mL) to achieve non-overload and overload conditions in rat AM. The cells were exposed to 150 µL of increasing concentrations of P25 (1 to 40 µg/mL) or Printex 90 (1 to 20 µg/mL) in a black 96-well culture plate with clear bottom (Greiner Bio-One) and, after 4 additional days, were fixed in 100µL formaldehyde 3.6% for a minimum of 20 min. After rinsing twice with PBS, cell pictures were taken by contrast microscopy (ZEISS LSM 800, Jena, Germany) using a 63X water immersion objective. We assessed different height levels and observed that the vast majority of particles were effectively internalized by the AM, rather than remaining attached to the surface. Pictures were then processed via the ImageJ software 1.53t. A macro was created using a black color set threshold of 0.55 (P25) or 0.33 (Printex 90) to highlight the particles and calculate the % surface of cellular particles. For each tested dose, more than 130 cells were analyzed and the mean and median % volume of intracellular particles was calculated. Based on these results, we selected non-cytotoxic doses leading to non-overload (mean and median % volume of particles < 6%) and overload (mean and median % volume of particles > 6%) conditions for each particle (Table S1). These nominal doses determined in rat AM were used for rat and human experiments as we considered that differences in cell volume or uptake

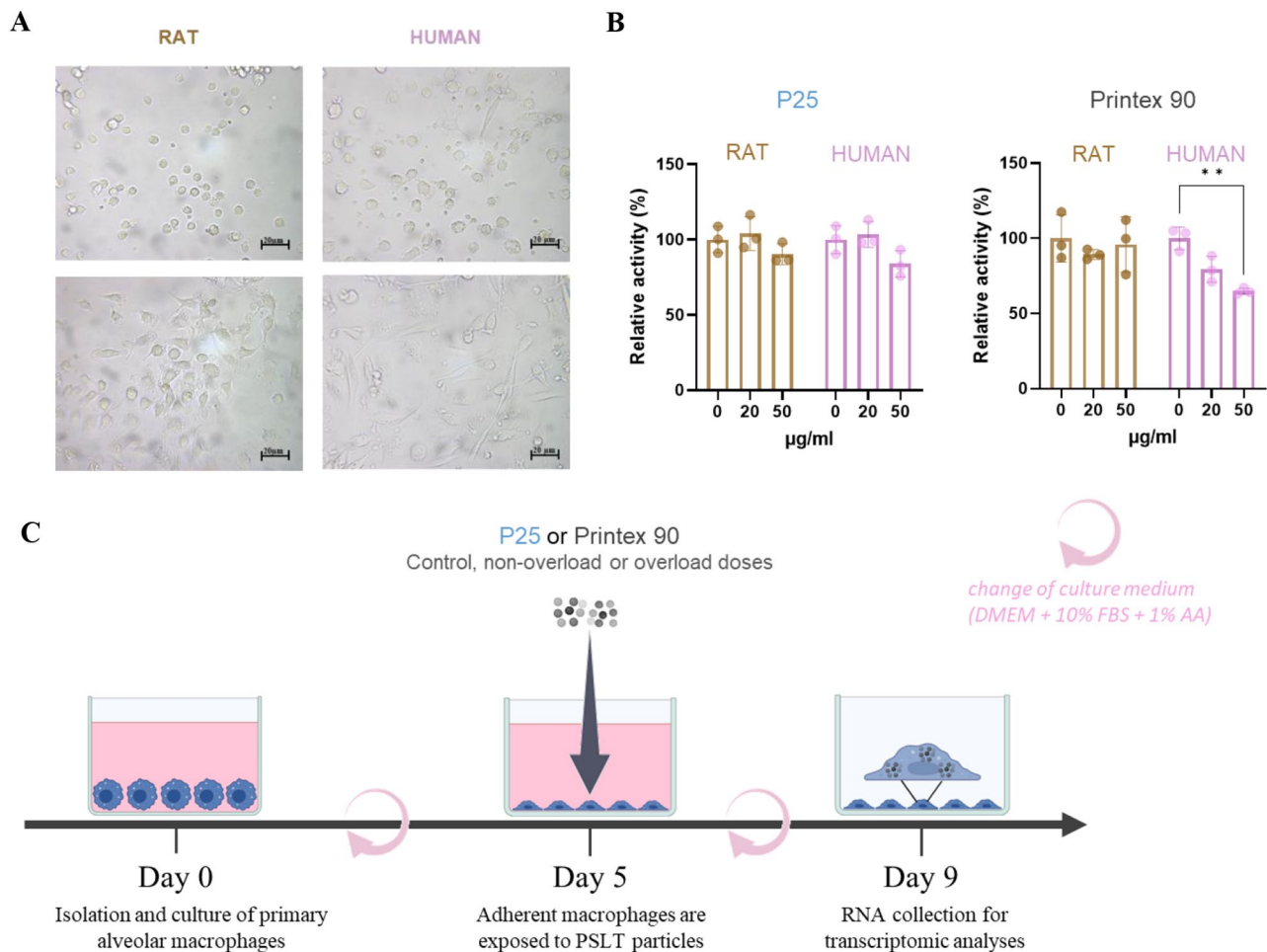


Fig. 1 Experimental design. **(A)** Pictures of primary AM from rat and human after 1 or 5 days of culture in DMEM supplemented with 10% FBS and 1% AA. Pictures were taken at 500X magnification with a camera placed on an optical invertoscope. **(B)** Rat and human AM were exposed to increasing doses of P25 or Printex 90 particles for 4 days. The number of live cells was determined with the WST-1 assay. Results are expressed as percentage of the control (0 $\mu\text{g/ml}$). Values are mean \pm SD from three technical replicates in a single experiment ($N=1$; $n=3$). For each particle, the data were compared by a two-way ANOVA followed by a post-hoc Dunnett test (treatment vs. control). $**p < 0.01$. **(C)** Timeline of culture and exposure of primary AM. Primary AM were isolated from rat or human via broncho-alveolar lavage and cultured in DMEM supplemented with 10% FBS and 1% AA. After 5 days of culture, AM, which have become adherent and exhibited pseudopods, were exposed to control, non-overload or overload doses of P25 or Printex 90 particles for 4 days. Between each step, the culture medium was changed every 2 or 3 days

rate may account for species differences in responses, and should not be erased by the experimental design. In addition, this approach allowed to reduce the number of cells and animals used.

Because the number of cells collected from a single rat was insufficient to extract an appropriate amount of RNA for HTS analyses, we pooled AM from several animals. Rat HTS analyses were performed on three technical replicates of pooled cells for each tested condition ($n=3$). To examine repeatability, two HTS independent experiments were performed ($N=2$). Due to practical limitations, human HTS analyses were performed on three biological replicates (one replicate = one volunteer, $n=3$) for each tested condition, in one experiment ($N=1$) (Fig. 2A).

RNA extraction

After appropriate dilution in complete culture medium, primary rat and human AM were exposed for 4 days to 500 μL of control, non-overload or overload conditions of P25 or Printex 90 in a 48-well culture plate. For RT-qPCR analyses and for the first HTS experiment in rat AM, total RNA was isolated by liquid-phase separation with TriPure Isolation Reagent according to manufacturer's instructions (Roche). For the second rat HTS experiment, and for the human experiment, an on-column extraction was performed using the RNeasy Mini Kits (Cat. 74106, Qiagen, Hilden, Germany) following the manufacturer's instructions. Residual DNA was removed by on-column DNase digestion using the RNase-Free DNase Set (Cat. 79254, Qiagen).

High-throughput RNA sequencing

RNA extracts corresponding to control, non-overload and overload doses were quantified with a Qubit fluorometer (Invitrogen, Gent, Belgium) using a Qubit RNA HS Assay kit. RNA quality and integrity were assessed

using the Agilent RNA 6000 Nano kit with an Agilent Bioanalyzer. Sequencing libraries were prepared using the KAPA RNA HyperPrep Kit with RiboErase for the Illumina platform (Kapabio Systems, Massachusetts, USA) using the standard protocol. After equimolar

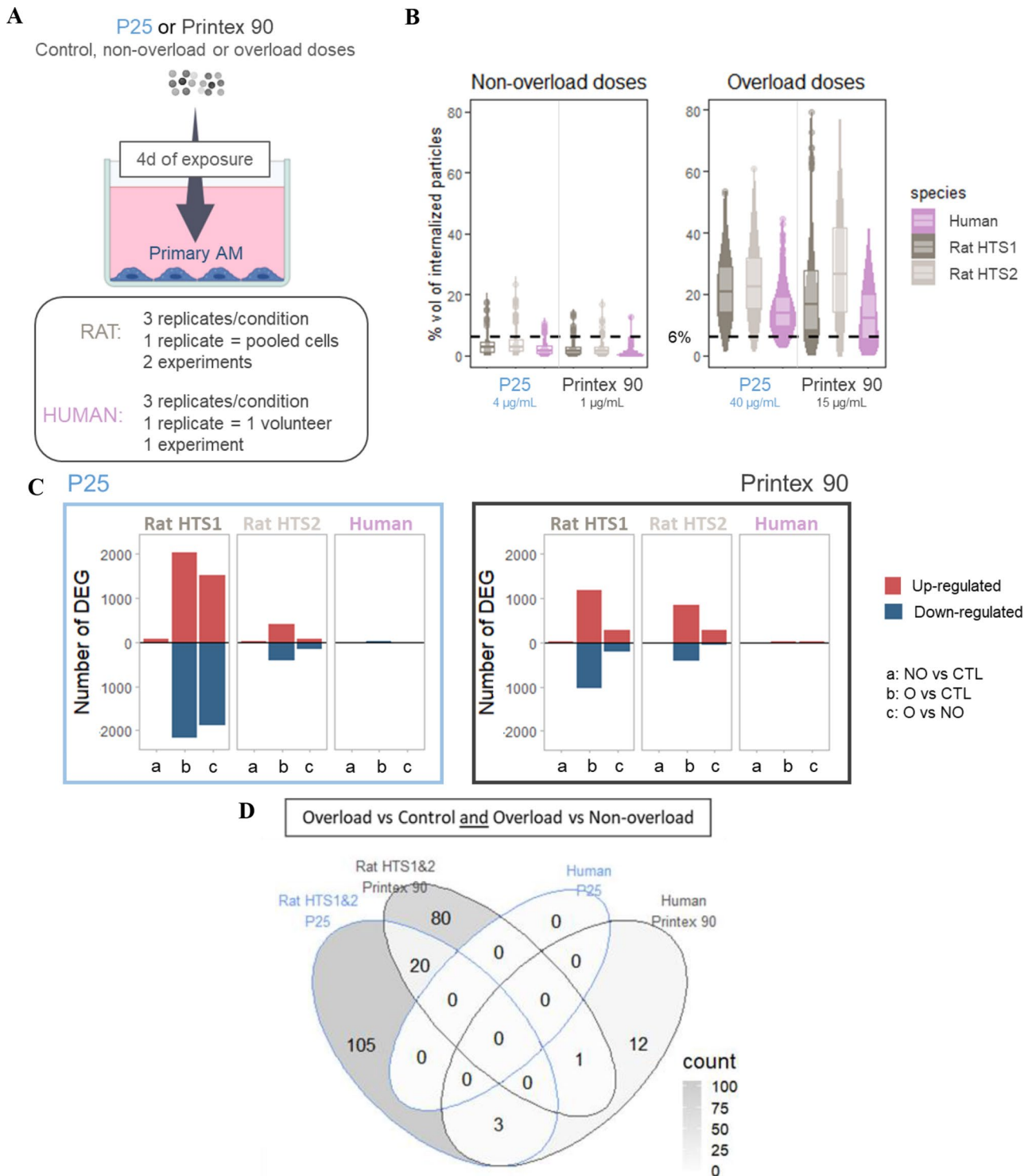


Fig. 2 (See legend on next page.)

(See figure on previous page.)

Fig. 2 Gene expression in rat and human AM following four days of exposure to P25 or Printex 90 particles. **(A)** Primary AM were isolated from rats or humans and exposed to control, non-overload or overload conditions of P25 or Printex 90 particles for four days. The HTS analyses were performed on 3 replicates from pooled AM for rats and on 3 biological replicates for humans. For rat AM, two experiments were performed. **(B)** Violin plot and box plot representing the percentage volume distribution of particles accumulated in rat and human AM, four days after exposure to rat non-overload or overload doses of P25 or Printex 90, as assessed by contrast microscopy. The boxplots represent the 25th and 75th percentiles with the median in the middle. The dotted line represents a volume of 6%. For each particle, and following Morrow's hypothesis [6], the selected doses led to non-overload (<6%) and overload (>6%) conditions in the AM of each species. **(C)** Comparison of the total number of differentially expressed genes (DEG, FDR < 0.05), up- or down-regulated, for each condition comparison in rat (first or second HTS experiment) and human AM. CTL = Control, NO = Non-overload, O = Overload. **(D)** Venn diagram of unique and shared genes significantly differentially expressed under overload conditions (comparing to control and non-overload conditions) between rat AM from the first and second HTS experiment (Rat HTS1&2) and human AM exposed to P25 or Printex 90 particles

pooling, libraries were sequenced on a Novaseq 6000 Illumina platform. A minimum of 25 M paired-end reads (2×100 bp) were generated per sample.

Libraries were prepared starting from 150 ng of total RNA from each exposure condition for each particle using the KAPA RNA HyperPrep Kit with RiboErase (HMR) (KAPA Biosystems, KK8560) following the manufacturer's recommendations (KR1351 – v1.16). Libraries were then equimolarly pooled and sequenced on a single lane on a Novaseq 6000 Illumina platform. A minimum of 25 M paired-end reads (2×100 bp) were generated per sample.

Bioinformatics

All sequencing data were analyzed using the Automated Reproducible MODular workflow for preprocessing and differential analysis of HTS data (ARMOR v1.5.4) pipeline [19]. In this pipeline, reads underwent a quality check using FastQC (Babraham Bioinformatics). Quantification and quality control results were summarized in a MultiQC report before being mapped using Salmon [20] to the transcriptome index which was built using all Ensembl cDNA sequences obtained in the *Rattus norvegicus.mRatBN7.2.cdna.all.fa* (Rat) and *Homo sapiens.GRCh38.cdna.all.fa* (Human). Then, estimated transcript abundances from Salmon were imported into R version 4.1.1 using the tximeta package [21] and analyzed for differential gene expression with edgeR [22]. Genes showing differences in expression between the different exposure conditions were identified for each particle and species separately. Given the distinct experimental designs for rat and human AM, the statistical tests were adapted accordingly for each species. The absolute expression difference between two conditions was calculated for each gene as a \log_2 fold-change (logFC). The statistical significance of this difference was then calculated as a false discovery rate (FDR). A multiple test correction of the p-value was performed in order to control the FDR at a level of 0.05. When gene modulations were compared between particles (P25 vs. Printex 90) or species (rat vs. human), Pearson correlation coefficient R and intraclass correlation coefficient ICC between the corresponding logFC

were computed to assess the correlation and the concordance, respectively [23]. Raw and processed HTS data were deposited and made publicly available on the Gene Expression Omnibus (First rat experiment: GSE271469, Second rat experiment: GSE272350, Human experiment: GSE273470).

RT-qPCR

For each particle, RT-qPCR was performed on 5 biological replicates of rat AM exposed for 4 days to control, non-overload or overload doses. RNA extracts (13.5 μ L) were reverse transcribed using random hexamers and M-MLV reverse transcriptase (Invitrogen, MA, USA) in a final volume of 25 μ L. PCR was performed on 5-fold diluted first-strand cDNA in sterile UltraPure® water (Invitrogen). Probe PCR reactions were prepared according to manufacturer's guidelines (Bio-Rad laboratories, CA, USA). Gene of interest were amplified and analyzed in duplex with the housekeeping gene (*Rplp0*). SsoAdvanced Universal Supermix (10 μ L) and primePCR probes ($2 \times 1 \mu$ L) were added to samples (4 μ L) and 20 μ L were loaded in a 96-well PCR plate. Probe references are listed in Table S3. PCR was performed using a StepOne-Plus™ Real-Time PCR system (Applied Biosystems™, MA, USA) with 40 amplification cycles of 5 s at 95 °C and 30 s at 60 °C. For each sample, Ct values were assigned using a threshold level determined by the StepOne™ Software v2.3 (Applied Biosystems). Relative differences in RNA expression among exposure conditions were assessed by the comparative Ct method. Briefly, Ct values were first normalized to that of the reference gene *Rplp0* in the same sample ($\Delta Ct = Ct_{\text{interest_gene}} - Ct_{\text{reference_gene}}$). The statistical significance of ΔCt values was then assessed on R version 4.1.1 by a linear mixed effect model with the rats as random effect. Differences with p-value < 0.05 were considered statistically significant. Then, ΔCt values were normalized to control group ($\Delta \Delta Ct = \Delta Ct_{\text{control_mean}} - \Delta Ct_{\text{samples}}$), giving the relative \log_2 fold-changes.

Ethics declaration

The collection of animal AM was approved by the Ethical Committee for Animal Experimentation at the

Health Science Sector, UCLouvain, Brussels, Belgium (No LA1230312) while the collection of human AM was approved by the local ethical committee of Cliniques universitaires St-Luc (Ref. 2017/04)AN/010). All volunteers gave signed informed consent.

Results

Exposure conditions

To analyze the transcriptomic responses of rat and human AM, we selected specific forms of TiO₂ (P25) and CB (Printex 90) particles, which had induced

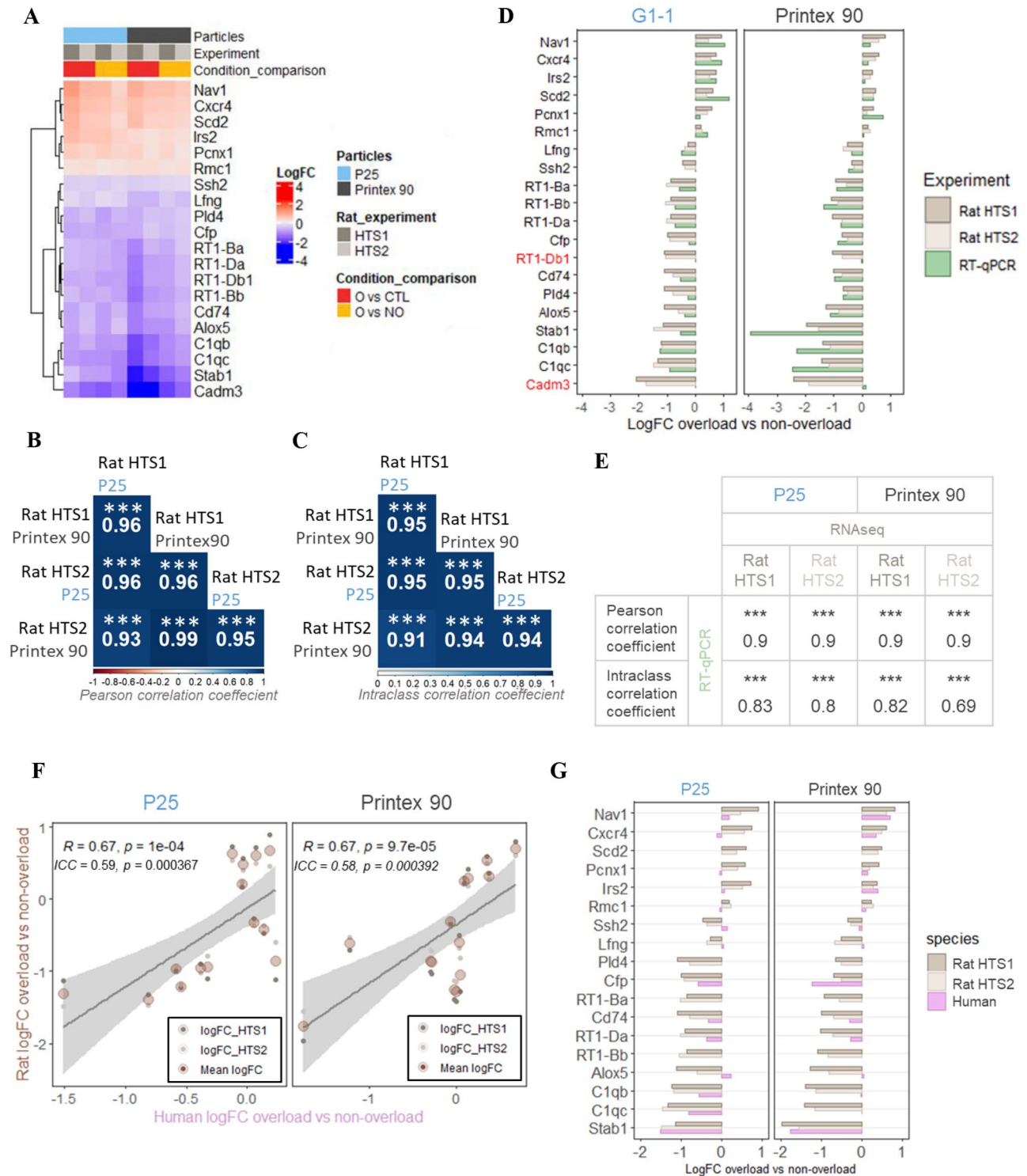


Fig. 3 (See legend on next page.)

(See figure on previous page.)

Fig. 3 Differentially expressed genes in rat AM following overload exposure to P25 or Printex 90 particles. **A-D.** Representation of the 20 genes significantly differentially expressed in the AM in both rat experiments following overload of P25 and Printex 90 particles. **A.** Heatmap representing the logFC between overload (O) and control (CTL) or overload and non-overload (NO) conditions in rat (first and second HTS experiment) AM exposed to P25 or Printex 90 particles. The 20 genes were modulated in the same direction comparing the conditions, experiments and particles. **B-C.** Correlation tables representing the Pearson correlation coefficient (**B**) or the intraclass correlation coefficient (**C**) reflecting the very strong positive correlation or concordance of the logFC (overload vs. non-overload conditions) of the 20 genes between both rat HTS experiments and both tested particles. Stars indicate significant correlation: $***p < 0.001$. **D.** Barplot representing the logFC between overload and non-overload conditions of the 20 genes comparing rat HTS analyses (first and second HTS experiment) and RT-qPCR analyses. RT-qPCR analyses were performed on 5 rat biological replicates. All genes, except *Cadm3* and *RT1-Db1* (in red), were similarly modulated comparing HTS and RT-qPCR analyses, after P25 and Printex 90 overload. **E-G.** Representation of the 18 genes (20 genes minus *Cadm3* and *RT1-Db1*) confirmed to be differentially expressed in rat AM under P25 and Printex 90 overload. **E.** Correlation table presenting the Pearson correlation coefficient or the intraclass correlation coefficient reflecting the strong positive correlation or concordance of the logFC (overload vs. non-overload conditions) of the 18 genes between rat HTS experiments and RT-qPCR analyses. Stars indicate significant correlation: $***p < 0.001$. **F.** Scatterplots comparing logFC values (overload vs. non-overload) between rat and human AM exposed to P25 or Printex 90 particles. Each dot represents one of the 18 genes. The small dots represent the logFC of each HTS experiment in rat AM while the big dots represent the mean of logFC of the two rat experiments. Each regression line indicates the linear relationship between the logFC of rat and human AM. The correlation degree between rat and human logFC was calculated by Pearson correlation coefficient R and the concordance of the values was calculated by the intraclass correlation coefficient ICC. A p -value < 0.05 indicates a significant correlation. **G.** Barplot representing the logFC (overload vs. non-overload conditions) of the 18 genes in rat (first and second HTS experiment) and human AM exposed to P25 or Printex 90 particles. Gene names are from reference genome *rattus norvegicus*

inflammatory and carcinogenic lung responses in experimental rats [3, 4]. We assessed the transcriptomic response after four days of particle exposure to minimize the possible acute response induced by the delivery of an acute bolus dose of particles in vitro, which would be non-specific and non-relevant for our study objectives. The cells were exposed to doses leading to AM overload or non-overload; the latter being included to subtract responses not specifically associated to particle overload (Fig. 2A). Based on the Morrow hypothesis [6], lung overload is initiated when rat AM have accumulated a volume of particles greater than 6% of their cell volume. Thus, exposure doses (expressed in $\mu\text{g}/\text{mL}$) leading to a % volume of intracellular particles below or above 6% were determined to achieve AM non-overload or overload conditions, respectively. Based on preliminary experiments, we selected exposure doses achieving these conditions in rat AM as being 4 and 40 $\mu\text{g}/\text{mL}$ for P25 and 1 and 15 $\mu\text{g}/\text{mL}$ for Printex 90. The same doses were used for exposing human AM (Table S1). The selected doses were not cytotoxic in AM from both species (Fig. 1B). The mean and median % volume of cellular particles was lower in human compared to rat AM (Fig. 2B and Table S1).

Rat AM were more responsive to particle overload than human AM

About 15,000 genes were expressed in the AM of both species in all tested conditions. Under particle overload, rat AM were markedly more responsive than human AM. Hundreds (second experiment) to thousands (first experiment) of genes were significantly differentially expressed ($\text{FDR} < 0.05$), when comparing control and/or non-overload doses to overload doses (Fig. 2C). Despite this difference in number of differentially expressed genes (DEG) between both rat experiments, 128 (P25) and 101 genes

(Printex 90) were significantly and similarly modulated in rat AM ($N=2$) when comparing overload conditions to both control *and* non-overload conditions (Fig. 2D and S2). Among these genes, 20 were commonly modulated by both PSLT particles (Figs. 2D and 3A). In human AM, no gene was statistically significantly modulated by overload of P25, while 16 genes were statistically significantly differentially expressed by Printex 90 under overload conditions (Figs. 2D and 4A). Among these 16 DEG, three were also significantly modulated in rat AM exposed to overload doses of P25 and one of them was significantly modulated in rat AM exposed to overload doses of Printex 90 (Fig. 2D).

Eighteen genes were identified as markers of P25 and printex 90 particle overload in rat AM

The magnitude and direction of gene expression changes (logFC) between overload and non-overload conditions were used to analyze and compare gene modulations across particles and species. The 20 genes modulated in rat AM by P25 and by Printex 90 overload were very strongly and significantly modulated in the same way when comparing the two rat experiments and particles ($R > 0.93$ and $\text{ICC} > 0.91$) (Figs. 3A-C). To confirm these sequencing data, real-time quantitative polymerase chain reaction (RT-qPCR) analyses were performed on AM isolated from rat biological replicates ($n=5$ rats/particle). The modulations of the 20 genes, as recorded by RT-qPCR analyses, were similar to those observed in HTS analyses, except for two genes (*Cadm3* and *RT1-Db1*) (Figs. 3D and S3). The modulation of the remaining 18 genes was strongly positively correlated when comparing HTS and RT-qPCR analyses (Fig. 3E). Overall, these results indicate that the 18 genes identified in rat AM provide a robust signature of P25 and Printex 90 overload in this in vitro model.

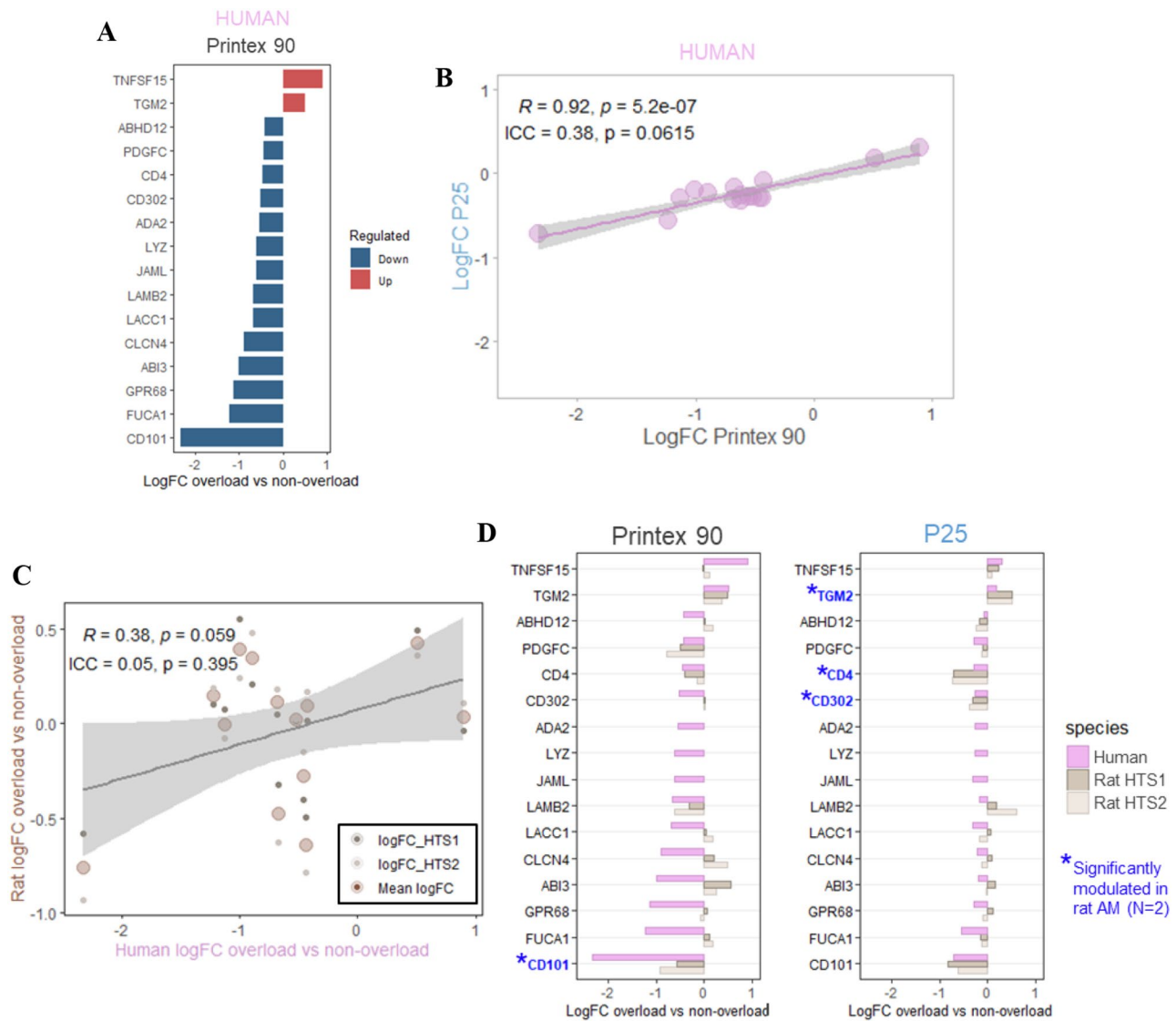


Fig. 4 Differentially expressed genes in human AM following overload exposure to Printex 90 particles. **A-D**. Representation of the 16 genes significantly differentially expressed in human AM exposed to Printex 90 overload. **A**. Barplot representing the logFC (overload vs. non-overload conditions) of the 16 genes in human AM. In red are the up-regulated genes and in blue the down-regulated genes. **B-C**. Scatterplots comparing logFC values (overload vs. non-overload) between P25 and Printex 90 in human AM (**B**) or between rat and human AM exposed to Printex 90 particles (**C**). Each dot represents one of the 16 genes. The small dots represent the logFC of each rat HTS experiment while the big dots represent the mean of logFC of the two rat experiments (**C**). Each regression line indicates the linear relationship between the logFC. The correlation degree between logFC was calculated by Pearson correlation coefficient R and the concordance of the values was calculated by the intraclass correlation coefficient ICC . A p -value < 0.05 indicates a significant correlation. **D**. Barplot representing the logFC (overload vs. non-overload conditions) of the 16 genes in rat (first and second HTS experiment) and human AM exposed to Printex 90 or P25 particles. The blue stars highlight genes, which were also significantly modulated in rat AM by overload conditions of Printex 90 or P25. Gene names are from reference genome Homo sapiens

The in vitro signature of P25 and printex 90 particle overload in rat AM was similarly modulated in human AM but with a lower amplitude

The amplitude of variation (logFC) under overload conditions (vs. non-overload) of the rat DEG was then compared between rat and human AM. *RT1-Ba* and

Scd2 rat genes have no direct (1:1) orthologous genes in humans and, the rat genes *Pld4* and *RT1-Bb* were not expressed in human cells. The logFC of the 14 orthologous/expressed genes in human AM was positively correlated with the logFC in rat AM (Fig. 3F). However, for most of the 14 genes, which were modulated in the same

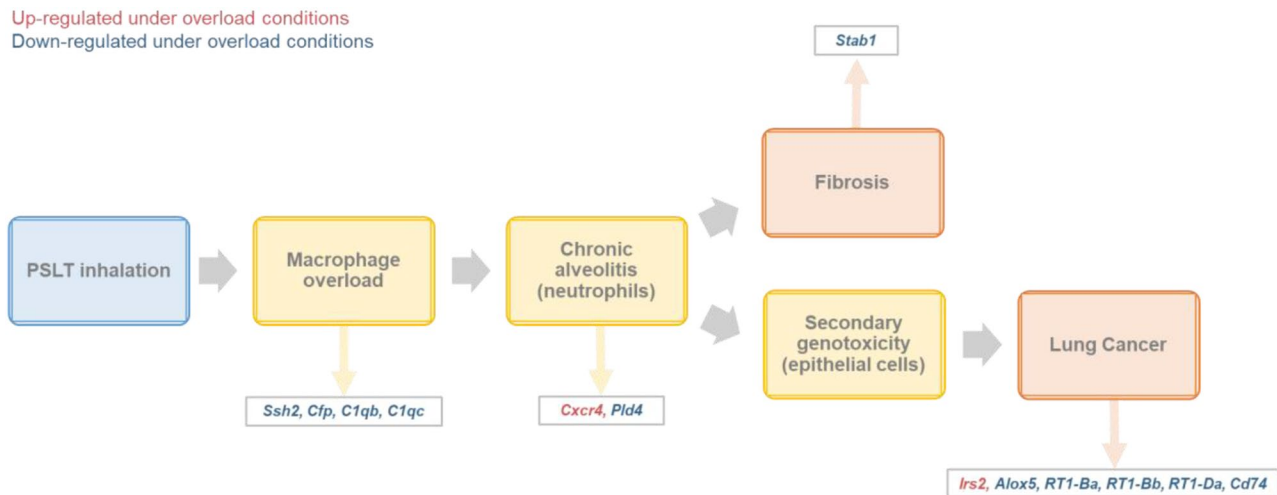


Fig. 5 Relationship between the proposed rat adverse outcome pathway. [9] and genes modulated by particle overload in rat AM. The large rectangles represent the different proposed key events linked to high exposure to PSLT particles in rats, leading to lung adverse outcomes. The grey small rectangles represent the genes significantly modulated by P25 and Printex 90 particle overload in rat AM

direction in both species, the amplitude of gene modulations in human AM was markedly lower compared to rat AM (on average 1.3 to 1.5 fold lower for both particles), and logFC were non-significant in human AM (Figs. 3G and S4). Thus, these results highlight similarities in gene modulation between rat and human AM exposed to particle overload, albeit with largely different sensitivities.

Sixteen genes were significantly modulated by printex 90 overload in human AM

Overload (vs. control and non-overload) of Printex 90 particles induced a significant modulation of 16 genes in human AM (Figs. 2D and 4A). Although these genes were not significantly modulated by P25 particle overload in human AM, the logFC of P25 and Printex 90 particles were very strongly positively correlated ($R=0.92$) but the magnitude of gene modulation was lower with P25 (ICC=0.38, on average 1.5 fold lower) (Fig. 4B). Comparing rat and human AM after Printex 90 particle overload, the modulations of the 16 genes were slightly positively but non-significantly correlated (Fig. 4C). Of the 16 genes, four were modulated in the same way by P25 only (*CD302*), or by P25 and Printex 90 (*TGM2*, *CD4* and *CD101*) particle overload in rat compared to human AM (Fig. 4D). All these genes were significantly modulated in rat AM exposed to overload of P25 (*CD302*, *TGM2* and *CD4*) or Printex 90 (*CD101*) particles (Fig. 4D and S5). However, among these 16 modulated human genes, some were modulated in opposite ways in rat AM (Figs. 4C-D and S5), did not have a direct (1:1) orthologous gene in rats (*ADA2* and *JAML*) or were not expressed in rat AM (*LYZ*). Overall, these results suggest that, despite some relation between both species, Printex 90 and P25 overload seemed to induce specific responses in human AM.

Discussion

This is the first study to examine the responses to particle overload in AM from rats and humans. The use of two different exposure doses, non-overload and overload, enabled us to isolate responses specific to AM overload. The particles used, their size and granulometry were relevant as they were similar to those used in chronic inhalation studies in which inflammatory and carcinogenic lung responses were recorded in rats [3, 4]. Furthermore, this study uniquely investigated particle exposure after 4 days of exposure, in contrast to most in vitro studies which typically focus on acute exposures (max. 24 h). This approach provided a relevant evaluation of the transcriptomic responses in the context of lung overload and its associated adverse outcomes.

Despite a great difference in the number of DEG between the two HTS experiments on rat AM, which may be explained by the different extraction methods [24] or by technical/batch biases [25], common gene modulations were observed in both experiments. Among these common genes, eighteen were specifically modulated under overload conditions by both P25 and Printex 90 particles. These genes were modulated in the same way in the two rat experiments with the two particles tested, and these modulations were confirmed by RT-qPCR analyses on 5 biological replicates. Overall, this response profile thus appears robust and specific to in vitro overload in rat AM.

The known function/activity as well as the modulation direction (up- or down-regulation) of 13 of these 18 genes can be related to the proposed adverse outcome pathway (AOP) for lung overload in the rat [9] (Fig. 5). Among these, *Ssh2*, a protein phosphatase involved in the regulation of actin filaments and thus cell mobility, was

down-regulated [26]. Genes belonging to the complement pathway (*Cfp*, *C1qb* and *C1qc*) were also down-regulated. These genes are important for efferocytosis, the phagocytosis of apoptotic cells [27, 28]. Impairment in efferocytic activity can lead to the accumulation of cellular debris and is related to chronic inflammatory diseases [29]. Efferocytosis impairment in macrophages has already been observed with particulate matter of air pollution and silica particles [30, 31]. In addition, *Cfp* is also involved in the phagocytosis of carbon nanotubes [32]. As overloaded macrophages show a reduction in their mobile and phagocytic activity in vivo [6, 33], the reduced expression of these genes contributes to validate our in vitro model to study overload. The up-regulated *Cxcr4* gene, codes for a chemokine receptor for Cxcl12. This complex can activate inflammatory signaling pathways such as mitogen-activated protein kinase (MAPK) and nuclear factor- κ B (NF- κ B), favoring the recruitment of inflammatory cells, including neutrophils [34]. Phospholipase D Family Member 4 (*Pld4*) is an exonuclease that cleaves single-stranded (ss) nucleic acids. Increase in ssDNA/RNA can activate nucleic-acid sensors, favoring autoimmune reactions [35]. Stabilin-1 (*Stab1*), a scavenger receptor involved in the clearance of fibrosis-related proteins, was down-regulated, suggesting a potential link to fibrosis development [36, 37]. TiO₂ nanoparticles highly reduce the expression and production of Stabilin-1 in primary human macrophages [37]. Additionally, *Irs2*, *Alox5* and genes belonging to the MHC class II protein complex (*RT1-Ba*, *RT1-Bb*, *RT1-Da*, *Cd74*) are modulated in tumor-associated macrophages. Up-regulation of *Irs2* favors a metabolic switch of macrophages to aerobic glycolysis, which, in turn, promotes the release of lactate, the fuel required by tumor cells [38, 39]. The down-regulation of *Alox5* and MHCII genes decreases the recruitment and activation of T lymphocytes, which can favor tumor growth [40–43]. This, however, contrasts with the down-regulation of *Stab1*, which is thought to have immunosuppressive activity [44]. Thus, the gene modulations observed in rat AM after P25 and Printex 90 overload in vitro appear related to the adverse outcomes reported previously under lung overload conditions in vivo in rats. These findings provide novel insights into the underlying mechanisms of lung adverse outcomes observed in vivo in rats after exposure to high doses of P25 or Printex 90 particles (Fig. 5).

We do not know yet if a similar modulation of this limited group of genes occurs and has an impact in vivo in rats. A previous study [43] identified a 15-gene signature in rat lungs exposed to high doses of Printex 90 and crystalline silica (DQ-12), absent in lower doses of Printex 90 or P25. However, as this signature was derived from comparisons with DQ-12, it may not be specific to PSLT overload, and none of these genes were

found in our study [45]. Moreover, whether these effects can be generalized to overload induced by other PSLT particles (talc, microplastics, tungsten carbide, or other grades of TiO₂ or CB particles) remains also unknown. P25 and Printex 90 particles are specific nanoforms of TiO₂ or CB particles which are much studied in inhalation toxicology but should not be considered as representative of other grades to which human populations could be exposed, mainly in occupational settings [15]. Additionally, serum in the culture medium may have led to a protein corona effect, potentially contributing to particle responses. Further studies are needed to explore this hypothesis.

The remaining five genes (out of the 18) have less clearly defined roles related to lung overload and adverse lung outcomes. *Nav1* encodes a sodium channel crucial for neuronal migration [46]. *Rmc1* regulates the MON1-CCZ1 complex, which plays a role in endosomal trafficking and autophagy [47]. Pecanex1 (*Pcnx1*) primarily functions as a competitive endogenous RNA (ceRNA), though its precise role remains unclear. *Scd2* is involved in the synthesis of monounsaturated fatty acids and plays a crucial role in mouse development [48]. Finally, *Lfng*, a glycosyltransferase involved in Notch signaling, is implicated in neuronal development [49]. Further in-depth analyses of these genes in the context of lung overload may reveal novel associated functions.

Beyond shared responses, P25 and Printex 90 particles showed distinct gene expression changes under overload conditions in rat AM. Notably, Printex 90 exposure downregulated *Cyp1b1* and *Ahrr*, genes involved in Polycyclic Aromatic Hydrocarbon (PAH) metabolism. *Cyp1b1* expression has already been shown to be decreased with Printex 90 exposure in the absence of PAH, while PAH-coated Printex 90 increased its expression [50]. Additionally, P25 particle exposure induced gene expression changes indicative of macrophage metabolic reprogramming, similar to lipopolysaccharide (LPS) stimulation [51]. A detailed analysis of these genes was beyond the scope of this study, which focused on responses specific to AM overload induced by PSLT particles.

In terms of number of DEG and of amplitude of modulations (logFC), rat AM, under overload conditions, were markedly more responsive to P25 and Printex 90 particles compared to human AM. However, the modulations of the 18 genes, specifically and highly modulated in rat AM, was positively correlated with modulations in human AM under overload, both by P25 and by Printex 90. But the amplitude of modulation of these human genes was markedly lower compared to rat AM and, consequently, logFC were not statistically significant. The markedly higher response to overload observed in rat relatively to human AM might, in part, reflect the greater volume of human

compared to rat AM (5000 vs. 1000 μm^3 [52]), and be thus related to the higher % volume of cellular particles accumulated by rat AM following exposure to overload (Fig. 2B and Table S1). Exploring the responses of human AM to higher particle concentrations could provide valuable insights. However, this approach may be challenging, particularly for Printex 90, as 50 $\mu\text{g}/\text{mL}$ exposure already induced significant cytotoxicity (Fig. 1B). Additionally, these differences may also reflect a higher sensitivity to overload of the rat AM compared to human AM. Direct comparisons of species-specific sensitivity remain challenging. A previous study found that unique RNA molecules in mice regulate inflammation via the Notch pathway, a mechanism absent in humans, which may increase their susceptibility to cytokine storms during viral infections [53]. LPS-induced gene modulation also exhibits species-specific differences between mouse and human macrophages, though these disparities tend to fade over time [54]. In contrast, studies on acute lung injury have revealed strong genetic signature correlations across species (mouse, rat and human), particularly in neutrophil-driven inflammation [55].

We have thus identified, for the first time, common responses to particle overload between rat and human AM *in vitro*. Extrapolating these data to human *in vivo* responses is not evident, especially because, *in vivo*, humans and rats differ on several aspects, including deposition and retention of particles in the lung, composition of broncho-alveolar lavage cells, higher oxidative stress responses in rats due to the production of reactive nitrogen species, inflammatory responses as well as neoplastic lung lesions [9]. Moreover, we do not know whether transcriptomic responses observed in an *in vitro* AM model can be extrapolated to dynamic and interactive *in vivo* responses in the same species. Proteomic/metabolomic analyses or more complex *ex vivo/in vitro* models, involving other cell types such as activated AM, epithelial cells or fibroblasts, might be useful to further understand the toxicological relevance of lung overload in humans.

Besides the responses observed in rat AM, a 16 gene signature of P25 and Printex 90 overload was observed in human AM. These 16 genes were significantly modulated by Printex 90 particle overload, and their modulation correlated extremely well with P25 particle overload. Of the 16 genes, *ABI3*, *CD302*, *JAML*, *CD4* and *PDGFC* are linked to cell migration, cell mobility or phagocytic activity [56–61]. These genes were down-regulated under overload of Printex 90 particles, suggesting a decrease in mobility and phagocytic activity of human AM, relevant for lung overload [6, 33]. Down-regulation of *ABHD12*, *LACC1*, *CD101* and *ADA2* may be related to inflammatory responses, as these genes appear to regulate

adaptive and/or innate immunity [62–66]. Up-regulation of *TGM2* and *TNFSF15* is frequently linked to fibrosis development and inflammation. *TGM2* is a multifunctional enzyme leading to posttranslational modification of many substrates and is distributed ubiquitously inside and outside the cells [67]. *TNFSF15* is a member of tumor necrosis factor family and can activate signaling pathway such as MAPK and NF- κ B through the binding to its receptor, the death receptor 3 [68]. The modulation of inflammatory-related genes was not surprising, knowing that exposure to particles, and non-self-antigens in general, affects inflammatory responses of macrophages [30, 69, 70]. These responses were observed four days following the exposure to the particles, indicating a possible sustained inflammatory response. Although, four of the 16 human genes (*CD4*, *CD302*, *CD101* and *TGM2*) were significantly and similarly modulated with overload of either P25 or Printex 90 in rat AM, the overall responses seemed specific to human AM. Most of the genes were not similarly modulated in rat AM following P25 or Printex 90 particle overload. Again, it is not yet possible to know whether transcriptomic responses observed in an *in vitro* model with a single cell type can be extrapolated to *in vivo* responses. Further studies are needed, involving proteomic/metabolomic analyses or more complex *in vitro* models, to draw conclusions about the possible *in vivo* outcomes of exposure to P25 or Printex 90 particles in humans.

Like many other studies, the present one has both strengths (see above) and limitations. The experimental design used for rat (experimental replicates of pooled AM) and human AM (biological replicates) was different, influencing the variability of the data. Despite these differences, the response of the 18 genes identified in the rat appears robust in the two omic and one RT-qPCR experiments. This study focused on the *in vitro* responses of a single cell type, AM, which are central to the early key events associated with lung overload. However, *in vitro* systems inherently differ from the dynamic and interactive *in vivo* environment, which involves a complex interplay between multiple cell types, including epithelial cells, fibroblasts and inflammatory cells. To avoid the acute responses associated with bolus dosing, which are less relevant to *in vivo* lung overload, we used the same exposure duration (4 days) for both species. However, the temporal patterns of AM responses to overload may differ between species. This aspect was not captured in the present study due to the single time point analysis.

Conclusion

This study revealed common and distinct transcriptomic responses to AM overload between rat and human AM. Overall, human AM were markedly less responsive (lower number of DEG and logFC) than rat AM to P25

and Printex 90 overload. In rat AM, a robust 18 gene in vitro signature of P25 and Printex 90 particle overload was found. The modulations of these genes observed under in vitro overload can be functionally related to the in vivo responses recorded in rats with the same particles. A similar signature was observed in human AM, although with a markedly lower amplitude than in rat AM. In addition, a unique 16 gene signature of Printex 90 overload was observed in human AM, which was not recorded in rat cells. Further studies are required to determine if these results can be generalised to other PSLT particles.

Supplementary Information

The online version contains supplementary material available at <https://doi.org/10.1186/s12989-025-00624-x>.

Supplementary Material 1

Acknowledgements

The authors thank the human volunteers for their contribution to this study. The authors thank the BRIGHTcore team at VUB/UZ Brussels for their help with the RNA-seq analyses. They also thank the TDMA and ICBA teams for their advice and expertise. Finally, we would like to acknowledge the contribution of Rita Vanbever team from the Louvain Drug Research Institute (LDRI) at UCLouvain for their expert guidance in laser diffraction analyses.

Author contributions

L.P. performed the experiments, data analyses, co-supervised the experimental design, and wrote the manuscript. J.A. performed most of the bioinformatic analyses. B.B. helped with RNA-sequencing analyses. A.F. and C.P. provided human alveolar macrophages. Y.Y. and M.P. helped with the animal experiments. C.B. helped with confocal microscopy analyses. L.R. performed scanning electron microscopy analyses. C.P. performed N₂ adsorption analyses. F.H. and D.L. conceived, designed and supervised the work and wrote the manuscript.

Funding

This study was supported by the Titanium Dioxide Manufacturers Association (TDMA) and the International Carbon Black Association (ICBA).

Data availability

Sequence data that support the findings of this study have been deposited on the Gene Expression Omnibus (First rat experiment: GSE271469, Second rat experiment: GSE272350, Human experiment: GSE273470).

Declarations

Ethics approval and consent to participate

The collection of rat AM was approved by the Ethical Committee for Animal Experimentation at the Health Science Sector, UCLouvain, Brussels, Belgium (No LA1230312) while the collection of human AM was approved by the local ethical committee of Cliniques universitaires St-Luc (Ref. 2017/04JAN/010). All volunteers gave signed informed consent.

Consent for publication

Not applicable.

Competing interests

The authors declare no competing interests.

Author details

¹Louvain Centre for Toxicology and Applied Pharmacology, Institute of Experimental and Clinical Research, Université catholique de Louvain, Brussels, Belgium

²Centre de Technologies Moléculaires Appliquées, Institute of Experimental and Clinical Research, Université catholique de Louvain, Brussels, Belgium

³Pôle Pneumologie, ORL (Airways) et dermatologie (Skin), Institute of Experimental and Clinical Research, Université catholique de Louvain, Brussels, Belgium

⁴Department of Pneumology, Cliniques Universitaires St-Luc, Brussels, Belgium

⁵Secteur des Sciences de la santé, Université catholique de Louvain, Louvain-la-Neuve, Belgium

⁶IREC Imaging Platform (2IP; RRID:SCR_023378), Institute of Experimental and Clinical Research, Université Catholique de Louvain, Brussels, Belgium

⁷Institute of Mechanics, Materials and Civil Engineering, Université Catholique de Louvain, Louvain-la-Neuve, Belgium

⁸Department of Chemistry, University of Turin, Turin, Italy

Received: 29 October 2024 / Accepted: 4 April 2025

Published online: 25 April 2025

References

- Haider AJ, Jameel ZN, Al-Hussaini IHM. Review on: titanium dioxide applications. *Energy Procedia*. 2019;157:17–29.
- Okoye CO, Jones I, Zhu M, Zhang Z, Zhang D. Manufacturing of carbon black from spent tyre pyrolysis oil– A literature review. *J Clean Prod* 2021; 279.
- Lee KP, Trochimowicz HJ, Reinhardt CF. Pulmonary response of rats exposed to titanium dioxide (TiO₂) by inhalation for two years. *Toxicol Appl Pharmacol*. 1985;79:179–92.
- Heinrich U, Fuhst R, Rittinghausen S, Creutzenberg O, Bellmann B, Koch W, Levsen K. Chronic inhalation exposure of Wistar rats and two different strains of mice to diesel engine exhaust, carbon black, and titanium dioxide. *Inhalation Toxicol*. 1995;7:533–56.
- Mauderly JL, Snipes MB, Barr EB, Belinsky SA, Bond JA, Brooks AL, Chang IY, Cheng YS, Gillett NA, Griffith WC et al. Pulmonary toxicity of inhaled diesel exhaust and carbon black in chronically exposed rats. Part I: neoplastic and nonneoplastic lung lesions. *Res Rep Health Eff Inst* 1994: 1–75; discussion 77–97.
- Morrow PE. Possible mechanisms to explain dust overloading of the lungs. *Fundam Appl Toxicol*. 1988;10:369–84.
- Oberdorster G, Ferin J, Morrow PE. Volumetric loading of alveolar macrophages (AM): a possible basis for diminished AM-mediated particle clearance. *Exp Lung Res*. 1992;18:87–104.
- Driscoll KE, Borm PJA. Expert workshop on the hazards and risks of poorly soluble low toxicity particles. *Inhal Toxicol*. 2020;32:53–62.
- Bos PMJ, Gosens I, Geraets L, Delmaar C, Cassee FR. Pulmonary toxicity in rats following inhalation exposure to poorly soluble particles: the issue of impaired clearance and the relevance for human health hazard and risk assessment. *Regul Toxicol Pharmacol*. 2019;109:104498.
- Braakhuis HM, Gosens I, Heringa MB, Oomen AG, Vandebriel RJ, Groenewold M, Cassee FR. Mechanism of action of TiO₂(2): recommendations to reduce uncertainties related to carcinogenic potential. *Annu Rev Pharmacol Toxicol*. 2021;61:203–23.
- Bermudez E, Mangum JB, Wong BA, Asgharian B, Hext PM, Warheit DB, Everitt JI. Pulmonary responses of mice, rats, and hamsters to subchronic inhalation of ultrafine titanium dioxide particles. *Toxicol Sci*. 2004;77:347–57.
- Elder A, Gelein R, Finkelstein JN, Driscoll KE, Harkema J, Oberdorster G. Effects of subchronically inhaled carbon black in three species. I. Retention kinetics, lung inflammation, and histopathology. *Toxicol Sci*. 2005;88:614–29.
- Carter JM, Corson N, Driscoll KE, Elder A, Finkelstein JN, Harkema JN, Gelein R, Wade-Mercer P, Nguyen K, Oberdorster G. A comparative dose-related response of several key pro- and anti-inflammatory mediators in the lungs of rats, mice, and hamsters after subchronic inhalation of carbon black. *J Occup Environ Med*. 2006;48:1265–78.
- Schulte PA, Leso V, Niang M, Iavicoli I. Current state of knowledge on the health effects of engineered nanomaterials in workers: a systematic review of human studies and epidemiological investigations. *Scand J Work Environ Health*. 2019;45:217–38.
- IARC. IARC Monographs on the Evaluation of Carcinogenic Risks to Humans - Carbon Black, Titanium Dioxide, and Talc. Lyon, France; 2010.

16. Wallace J, Jackson GR, Kaluzhny Y, Ayehunie S, Lansley AB, Roper C, Hayden PJ. Evaluation of in vitro rat and human airway epithelial models for acute inhalation toxicity testing. *Toxicol Sci.* 2023;194:178–90.
17. Kienhuis AS, van de Poll MC, Wortelboer H, van Herwijnen M, Gottschalk R, Dejong CH, Boorsma A, Paulus RS, Kleinjans JC, Stierum RH, van Delft JH. Parallelogram approach using rat-human in vitro and rat in vivo toxicogenomics predicts acetaminophen-induced hepatotoxicity in humans. *Toxicol Sci.* 2009;107:544–52.
18. DeLooid GM, Cohen JM, Pyrgiotakis G, Demokritou P. Preparation, characterization, and in vitro dosimetry of dispersed, engineered nanomaterials. *Nat Protoc.* 2017;12:355–71.
19. Orjuela S, Huang R, Hembach KM, Robinson MD, Soneson C. ARMOR: an automated reproducible modular workflow for preprocessing and differential analysis of RNA-seq data. *G3 (Bethesda).* 2019;9:2089–96.
20. Cunningham F, Achuthan P, Akanni W, Allen J, Amode MR, Armean IM, Bennett R, Bhai J, Billis K, Boddu S, Cummins C, Davidson C, Dodiya KJ, Gall A, Giron CG, Gil L, Grego T, Haggerty L, Haskell E, Hourlier T, Izuogu OG, Janacek SH, Juettemann T, Kay M, Laird MR, Lavidas I, Liu Z, Loveland JE, Marugan JC, Maurel T, McMahon AC, Moore B, Morales J, Mudge JM, Nuhn M, Ogeh D, Parker A, Parton A, Patricio M, Abdul Salam AI, Schmitt BM, Schuilenburg H, Sheppard D, Sparrow H, Stapleton E, Szuba M, Taylor K, Threadgold G, Thormann A, Vullo A, Walts B, Winterbottom A, Zadissa A, Chakiachvili M, Frankish A, Hunt SE, Kostadima M, Langridge N, Martin FJ, Muffato M, Perry E, Ruffier M, Staines DM, Trevanion SJ, Aken BL, Yates AD, Zerbino DR, Flicke P. Ensembl 2019. *Nucleic Acids Res.* 2019;47:D745–51.
21. Soneson C, Love MI, Robinson MD. Differential analyses for RNA-seq: transcript-level estimates improve gene-level inferences. *F1000Res.* 2015;4:1521.
22. Robinson MD, McCarthy DJ, Smyth GK. EdgeR: a bioconductor package for differential expression analysis of digital gene expression data. *Bioinformatics.* 2010;26:139–40.
23. Liu J, Tang W, Chen G, Lu Y, Feng C, Tu XM. Correlation and agreement: overview and clarification of competing concepts and measures. *Shanghai Arch Psychiatry.* 2016;28:115–20.
24. Scholes AN, Lewis JA. Comparison of RNA isolation methods on RNA-Seq: implications for differential expression and meta-analyses. *BMC Genomics.* 2020;21:249.
25. Leek JT, Scharpf RB, Bravo HC, Simcha D, Langmead B, Johnson WE, Geman D, Baggerly K, Irizarry RA. Tackling the widespread and critical impact of batch effects in high-throughput data. *Nat Rev Genet.* 2010;11:733–9.
26. Tang W, Zhang Y, Xu W, Harden TK, Sondek J, Sun L, Li L, Wu D. A PLCbeta/PI3Kgamma-GSK3 signaling pathway regulates Cofilin phosphatase slingshot2 and neutrophil polarization and chemotaxis. *Dev Cell.* 2011;21:1038–50.
27. Kemper C, Hourcade DE, Properdin. New roles in pattern recognition and target clearance. *Mol Immunol.* 2008;45:4048–56.
28. Galvan MD, Greenlee-Wacker MC, Bohlson SS. C1q and phagocytosis: the perfect complement to a good meal. *J Leukoc Biol.* 2012;92:489–97.
29. McCubbrey AL, Curtis JL. Efferocytosis and lung disease. *Chest.* 2013;143:1750–7.
30. Hiraiwa K, van Eeden SF. Contribution of lung macrophages to the inflammatory responses induced by exposure to air pollutants. *Mediators Inflamm.* 2013;2013:619523.
31. Lescoat A, Ballerie A, Lelong M, Augagneur Y, Morzadec C, Jouneau S, Jégo P, Fardel O, Verhnet L, Lecureur V. Crystalline silica impairs efferocytosis abilities of human and mouse macrophages: implication for silica-Associated systemic sclerosis. *Front Immunol* 2020; 11.
32. Kouser L, Paudyal B, Kaur A, Stenbeck G, Jones LA, Abozaid SM, Stover CM, Flahaut E, Sim RB, Kishore U. Human Properdin opsonizes nanoparticles and triggers a potent Pro-inflammatory response by macrophages without involving complement activation. *Front Immunol.* 2018;9:131.
33. Renwick LC, Donaldson K, Clouter A. Impairment of alveolar macrophage phagocytosis by ultrafine particles. *Toxicol Appl Pharmacol.* 2001;172:119–27.
34. Tian X, Xie G, Xiao H, Ding F, Bao W, Zhang M. CXCR4 knockdown prevents inflammatory cytokine expression in macrophages by suppressing activation of MAPK and NF-kappaB signaling pathways. *Cell Biosci.* 2019;9:55.
35. Gavin AL, Huang D, Blane TR, Thinnies TC, Murakami Y, Fukui R, Miyake K, Nemazee D. Cleavage of DNA and RNA by PLD3 and PLD4 limits autoinflammatory triggering by multiple sensors. *Nat Commun.* 2021;12:5874.
36. Kzhyshkowska J, Krusell L. Cross-talk between endocytic clearance and secretion in macrophages. *Immunobiology.* 2009;214:576–93.
37. Silva-Bermudez LS, Sevastyanova TN, Schmutzmaier C, De La Torre C, Schumacher L, Kluter H, Kzhyshkowska J. Titanium nanoparticles enhance production and suppress Stabilin-1-Mediated clearance of GDF-15 in human primary macrophages. *Front Immunol.* 2021;12:760577.
38. Landis J, Shaw LM. Insulin receptor substrate 2-mediated phosphatidylinositol 3-kinase signaling selectively inhibits glycogen synthase kinase 3beta to regulate aerobic Glycolysis. *J Biol Chem.* 2014;289:18603–13.
39. Duncan-Moretti NM-B, Cd-C JH, Saldanha-Gama R, Paula-Neto HA, G GD, Barja-Fidalgo RLS. Aerobic Glycolysis is a metabolic requirement to maintain the M2-like polarization of tumor-associated macrophages. *Biochim Biophys Acta Mol Cell Res.* 2020;1867:118604.
40. Ringleb J, Strack E, Angioni C, Geisslinger G, Steinhilber D, Weigert A, Brune B. Apoptotic cancer cells suppress 5-Lipoxygenase in Tumor-Associated macrophages. *J Immunol.* 2018;200:857–68.
41. Poczbott JM, Nguyen TT, Hanson D, Li H, Sippel TR, Weiser-Evans MC, Gijon M, Murphy RC, Nemenoff RA. Deletion of 5-Lipoxygenase in the tumor micro-environment promotes lung cancer progression and metastasis through regulating T cell recruitment. *J Immunol.* 2016;196:891–901.
42. Wang B, Li Q, Qin L, Zhao S, Wang J, Chen X. Transition of tumor-associated macrophages from MHC class II(hi) to MHC class II(low) mediates tumor progression in mice. *BMC Immunol.* 2011;12:43.
43. Haabeth OA, Tveita AA, Fauskanger M, Schjesvold F, Lørvik KB, Hofgaard PO, Omholt H, Munthe LA, Dembic Z, Corthay A, Bogen B. How do CD4(+) T cells detect and eliminate tumor cells that either lack or express MHC class II molecules? *Front Immunol.* 2014;5:174.
44. Hollmen M, Figueiredo CR, Jalkanen S. New tools to prevent cancer growth and spread: a 'clever' approach. *Br J Cancer.* 2020;123:501–9.
45. Valentino SA, Seidel C, Lorcin M, Sebillaud S, Wolff H, Grossmann S, Viton S, Nunge H, Saarimaki LA, Greco D, Cosnier F, Gate L. Identification of a gene signature predicting (Nano)Particle-Induced adverse lung outcome in rats. *Int J Mol Sci* 2023; 24.
46. Martinez-Lopez MJ, Alcantara S, Mascaro C, Perez-Branguli F, Ruiz-Lozano P, Maes T, Soriano E, Buesa C. Mouse neuron navigator 1, a novel microtubule-associated protein involved in neuronal migration. *Mol Cell Neurosci.* 2005;28:599–612.
47. Vaites LP, Paulo JA, Huttlin EL, Harper JW. Systematic analysis of human cells lacking ATG8 proteins uncovers roles for GABARAPs and the CCZ1/MON1 regulator C18orf8/RMC1 in macroautophagic and selective autophagic flux. *Mol Cell Biol* 2018; 38.
48. O'Neill LM, Guo CA, Ding F, Phang YX, Liu Z, Shamsuzzaman S, Ntambi JM. Stearoyl-CoA Desaturase-2 in murine development, metabolism, and disease. *Int J Mol Sci* 2020; 21.
49. Semerci F, Choi WT, Bajic A, Thakkar A, Encinas JM, Depreux F, Segil N, Groves AK, Maletic-Savatic M. Lunatic fringe-mediated Notch signaling regulates adult hippocampal neural stem cell maintenance. *Elife* 2017; 6.
50. Lindner K, Strobele M, Schlick S, Webering S, Jenckel A, Kopf J, Danov O, Sewald K, Buj C, Creutzenberg O, Tillmann T, Pohlmann G, Ernst H, Ziemann C, Huttmann G, Heine H, Bockhorn H, Hansen T, König P, Fehrenbach H. Biological effects of carbon black nanoparticles are changed by surface coating with polycyclic aromatic hydrocarbons. *Part Fibre Toxicol.* 2017;14:8.
51. Kelly B, O'Neill LA. Metabolic reprogramming in macrophages and dendritic cells in innate immunity. *Cell Res.* 2015;25:771–84.
52. Krombach F, Munzing S, Allmeling AM, Gerlach JT, Behr J, Dorger M. Cell size of alveolar macrophages: an interspecies comparison. *Environ Health Perspect.* 1997;105(Suppl 5):1261–3.
53. Ma H, Yang Y, Nie T, Yan R, Si Y, Wei J, Li M, Liu H, Ye W, Zhang H, Cheng L, Zhang L, Lv X, Luo L, Xu Z, Zhang X, Lei Y, Zhang F. Disparate macrophage responses are linked to infection outcome of Hantaan virus in humans or rodents. *Nat Commun.* 2024;15:438.
54. Schroder K, Irvine KM, Taylor MS, Bokil NJ, Le Cao KA, Masterman KA, Labzin LI, Semple CA, Kapetanovic R, Fairbairn L, Akalin A, Faulkner GJ, Baillie JK, Gongora M, Daub CO, Kawaji H, McLachlan GJ, Goldman N, Grimmond SM, Carninci P, Suzuki H, Hayashizaki Y, Lenhard B, Hume DA, Sweet MJ. Conservation and divergence in Toll-like receptor 4-regulated gene expression in primary human versus mouse macrophages. *Proc Natl Acad Sci U S A.* 2012;109:E944–953.
55. Sweeney TE, Lofgren S, Khatri P, Rogers AJ. Gene expression analysis to assess the relevance of rodent models to human lung injury. *Am J Respir Cell Mol Biol.* 2017;57:184–92.
56. Rottner K, Stradal TEB, Chen B. WAVE regulatory complex. *Curr Biol.* 2021;31:R512–7.
57. Kato M, Khan S, d'Aniello E, McDonald KJ, Hart DN. The novel endocytic and phagocytic C-Type lectin receptor DCL-1/CD302 on macrophages is

- colocalized with F-actin, suggesting a role in cell adhesion and migration. *J Immunol.* 2007;179:6052–63.
58. Guo YL, Bai R, Chen CX, Liu DQ, Liu Y, Zhang CY, Zen K. Role of junctional adhesion molecule-like protein in mediating monocyte transendothelial migration. *Arterioscler Thromb Vasc Biol.* 2009;29:75–83.
 59. Tomasi S, Li L, Hinske LC, Tomasi R, Amini M, Strauss G, Muller MB, Hirschberger S, Peterss S, Effinger D, Pogoda K, Kreth S, Hubner M. A functional network driven by MicroRNA-125a regulates monocyte trafficking in acute inflammation. *Int J Mol Sci* 2022; 23.
 60. Zhen A, Krutzik SR, Levin BR, Kasparian S, Zack JA, Kitchen SG, Silvestri G. CD4 ligation on human blood monocytes triggers macrophage differentiation and enhances HIV infection. *J Virol.* 2014;88:9934–46.
 61. Wagsater D, Zhu C, Bjorck HM, Eriksson P. Effects of PDGF-C and PDGF-D on monocyte migration and MMP-2 and MMP-9 expression. *Atherosclerosis.* 2009;202:415–23.
 62. Ogasawara D, Ichu TA, Jing H, Hulce JJ, Reed A, Ulanovskaya OA, Cravatt BF. Discovery and optimization of selective and in vivo active inhibitors of the lysophosphatidylserine lipase alpha/beta-Hydrolase Domain-Containing 12 (ABHD12). *J Med Chem.* 2019;62:1643–56.
 63. Wei Z, Oh J, Flavell RA, Crawford JM. LACC1 bridges NOS2 and polyamine metabolism in inflammatory macrophages. *Nature.* 2022;609:348–53.
 64. Schey R, Dornhoff H, Baier JL, Purtak M, Opoka R, Koller AK, Atreya R, Rau TT, Daniel C, Amann K, Bogdan C, Mattner J. CD101 inhibits the expansion of colitogenic T cells. *Mucosal Immunol.* 2016;9:1205–17.
 65. Blackburn MR. Too much of a good thing: adenosine overload in adenosine-deaminase-deficient mice. *Trends Pharmacol Sci.* 2003;24:66–70.
 66. Signa S, Bertoni A, Penco F, Caorsi R, Cafaro A, Cangemi G, Volpi S, Gattorno M, Schena F. Adenosine deaminase 2 deficiency (DADA2): A crosstalk between innate and adaptive immunity. *Front Immunol.* 2022;13:935957.
 67. Tatsukawa H, Hitomi K. Role of transglutaminase 2 in cell death, survival, and fibrosis. *Cells* 2021; 10.
 68. Xu WD, Li R, Huang AF. Role of TL1A in inflammatory autoimmune diseases: A comprehensive review. *Front Immunol.* 2022;13:891328.
 69. Kusaka T, Nakayama M, Nakamura K, Ishimiya M, Furusawa E, Ogasawara K. Effect of silica particle size on macrophage inflammatory responses. *PLoS ONE.* 2014;9:e92634.
 70. Chaplin DD. Overview of the immune response. *J Allergy Clin Immunol.* 2010;125:S3–23.

Publisher's note

Springer Nature remains neutral with regard to jurisdictional claims in published maps and institutional affiliations.